Hyperfine interaction in the Autler-Townes effect: The formation of bright, dark, and chameleon states

T. Kirova, A. Cinins, D. K. Efimov, M. Bruvelis, K. Miculis, N. N. Bezuglov, M. Auzinsh, I. I. Ryabtsev, and A. Ekers

Phys. Rev. A **96**, 043421 — Published 26 October 2017

DOI: 10.1103/PhysRevA.96.043421

Hyperfine interaction in the Autler-Townes effect: the formation of bright, dark, and chameleon states

T. Kirova[a], A. Cinins[a,b],* D. K. Efimov[c,b],† M. Bruvelis[b], K. Miculis[a,d], N. N. Bezuglov[c], M. Auzinsh[b], I. I. Ryabtsev[e,f], and A. Ekers[g]

[a] *University of Latvia, Institute of Atomic Physics and Spectroscopy, LV-1586 Riga, Latvia*
[b] *University of Latvia, Laser Centre, LV-1002, Riga, Latvia*
[c] *Saint Petersburg State University, 7/9 Universitetskaya nab., St. Petersburg, 199034 Russia*
[d] *Moscow State Engineering Physics Institute, 115409 Moscow, Russia*
[e] *Rzhanov Institute of Semiconductor Physics SB RAS, 630090 Novosibirsk, Russia*
[f] *Novosibirsk State University, Department of Physics, 630090 Novosibirsk, Russia*
[g] *King Abdullah University of Science and Technology (KAUST), Computer, Electrical and Mathematical Sciences and Engineering Division (CEMSE), Thuwal 23955-6900, Saudi Arabia*

(Dated: July 26, 2017)

This paper is devoted to clarifying the implications of hyperfine (HF) interaction in the formation of adiabatic (i.e., "laser-dressed") states and their expression in the Autler-Townes (AT) spectra. We first use the Morris-Shore model (J. R. Morris and B. W. Shore, Phys. Rev. A 27, 906 (1983) [1]) to illustrate how bright and dark states are formed in a simple reference system where closely spaced energy levels are coupled to a single state with a strong strong laser field with the respective Rabi frequency Ω_S. We then expand the simulations to realistic hyperfine level systems in Na atoms for a more general case when non-negligible HF interaction can be treated as a perturbation in the total system Hamiltonian. A numerical analysis of the adiabatic states that are formed by coupling of the $3p_{3/2}$ and $4d_{5/2}$ states by the strong laser field and probed by a weak laser field on the $3s_{1/2}$ – $3p_{3/2}$ transition yielded two important conclusions. First, the perturbation introduced by the HF interaction leads to observation of what we term "chameleon" states – states that change their appearance in the AT spectrum, behaving as bright states at small to moderate Ω_S, and fading from the spectrum similarly to dark states when Ω_S is much larger than the HF splitting of the $3p_{3/2}$ state. Secondly, excitation by the probe field from two different HF levels of the ground state allows one to address orthogonal sets of adiabatic states; this enables, with appropriate choice of Ω_S and the involved quantum states, a selective excitation of otherwise unresolved hyperfine levels in excited electronic states.

PACS numbers: 42.50.Hz, 32.80.Qk, 32.10.Fn, 31.15.-p

I. INTRODUCTION

Since the first study of microwave-radio frequency double resonance excitation of OCS molecules by Stanley Autler and Charles Townes more than half a century ago that gave raise to the term Autler-Townes (AT) effect [2], it has made a profound impact on the discovery and correct theoretical description of a large number of important quantum optics phenomena throughout the following decades. Yet, after careful examination of the existing scientific literature, we came to a realization that a clear understanding of the role and expression of hyperfine (HF) interaction in the AT effect is still missing, in particular in the case when the coupling strength of atoms or molecules with the laser field becomes comparable or exceeds the HF separations of energy levels.

Intuitively, it may be compelling to presume that a decoupling analogous to Paschen-Back effect upon interaction of hyperfine level systems with strong magnetic fields [3, 4] would take place when the Rabi frequency of light-atom interaction exceeds the HF interaction energy. However, after a more thorough thinking one can quickly realize that the dynamics of the adiabatic state formation complicates the matter and such analogy is at best superficial. The aim of this study is to clarify how exactly the HF interaction affects the formation of adiabatic states in the AT effect and how those states are expressed in the laser excitation spectra. In the weak excitation limit, the effects of partially resolved hyperfine structure on light-induced polarization of atoms have been studied in detail in [5]. Here, we are concerned with the effects of strong coupling on the formation of dark and bright states upon interaction of a hyperfine level system with coherent light fields. As will be shown below, the presence of the HF interaction introduces a third kind of states that, being neither strictly "dark" nor strictly "bright", exhibit a blend of features characteristic of bright and dark states that changes with the strength of the coupling field. For this latter property we term them the "chameleon" states.

Dark states play a crucial role in various schemes of quantum state manipulation by coherent radiation fields.

* arturs.cinins@lu.lv
† Present address: Instytut Fizyki im. Mariana Smoluchowskiego, Uniwersytet Jagielloński, 30-348 Kraków, Poland

The first interference experiment showing cancellation of absorption was performed by Fano [6] and it subsequently led to the idea of coherent population trapping (CPT) and "dark" state formation [7]. When one of the laser fields is much weaker than the other, the "dark" state coincides with a stable level in the ground state, where population is trapped, and the system exhibits electromagnetically induced transparency (EIT) [8]. The EIT and the related to it optical response of the absorbing medium have found numerous applications in controlling the group velocity of light [9, 10], quantum information storage [11, 12], quantum computing [13], magnetometers [14], and atomic clocks [15]. When two or more strong laser fields are used to guide the evolution of the dark state, one can realize the so called stimulated Raman adiabatic passage (STIRAP) technique [16] that enables a complete population transfer between quantum states and is now finding applications well beyond the realm of gas phase atomic physics, an account of which is given in the recent review [17].

Even though the usual theoretical approach to treat the formation of dressed states is based on two-level and three-level [18] excitation schemes, almost all realistic systems exhibit either a Zeeman sublevel structure or a hyperfine (HF) structure, or both. An experiment on AT effect in Li_2 molecules [19] has shown that under certain conditions Zeeman sublevels may be resolved and appear in the AT spectra as groups of peak-pairs corresponding to coupling of different sets of Zeeman sublevels.

The formation of dark states in excitation schemes consisting of more than three levels was first considered by Morris and Shore [1]. They applied the so-called Morris-Shore (MS) transformation [1, 20] to show that an excitation scheme with N_A degenerate (for instance, Zeeman) levels in the ground state and N_B degenerate levels in the excited state gives rise to $\min\{N_A, N_B\}$ pairs of bright MS states and $|N_A - N_B|$ dark MS states (see also Sect. III A).

In this paper we are concerned with the formation and spectral manifestation of adiabatic states formed via strong laser coupling of multiple hyperfine levels. One of the key questions is whether one can upfront disregard the HF interaction when the light-atom interaction Rabi frequency exceeds HF level separations, or are there more subtle effects in the formation of bright and dark states that are notably affected by parameters such as the HF quantum number F and the respective magnetic quantum number $M \equiv M_F$. In either case, we expect to be able to identify the effects of the HF interaction in the AT spectra. The analysis and interpretation of the latter are nontrivial due to the complexity added by introducing the HF structure to the atomic energy levels. We shall therefore proceed successively, starting with simplified model systems and advancing to analysis of a real-life example of a three-level ladder excitation scheme $3s_{1/2} - 3p_{3/2} - 4d_{5/2}$ in Na atoms (see Fig.5(a)) that is conveniently accessible for excitation and spectroscopic observation in the visible spectral range. In this scheme,

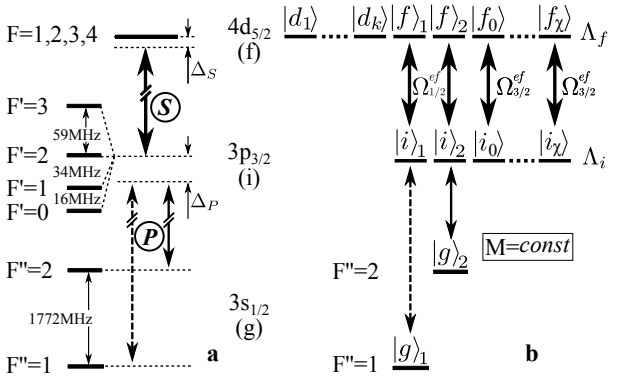

FIG. 1. (a) The considered excitation scheme in atomic sodium. The weak probe laser field P is scanned across the transition between the ground state g $3s_{1/2}$ ($F'' = 2$ or $F'' = 1$) and the intermediate state i $3p_{3/2}$, whereas the strong field S couples the intermediate state i to the final state f $4d_{5/2}$. (b) The same level scheme after Morris-Shore transformation in the HF basis with semi-broken HF coupling (see in Sect. V). The set of Bright $|f\rangle_{1,2}$, Chameleon $|f_{0\ldots\chi}\rangle$ and Dark $|d_{1\ldots k}\rangle$ states in the f-space Λ_f depends on the magnetic quantum number M (see Fig.6(a)-(c)). The index η that is used with states $|g, i, f\rangle_\eta$ is defined in Sect V as a double-index $\eta = F'', M$. In the current example it indicates only the quantum number F''. For example, for Zeeman sublevels with $M = 1$ there is one Chameleon ($\chi = 0$) and one Dark ($k = 1$) state, while $|g, i, f\rangle_1 \equiv |g, i, f\rangle_{1,1}$, $|g, i, f\rangle_2 \equiv |g, i, f\rangle_{2,1}$.

a strong laser field couples the $3p$ and $4d$ states, creating adiabatic (dressed) states [21] that are then probed by a weak laser field on the $3s - 3p$ transition.

In what follows we shall rely on the rotating wave approximation (RWA) [22], in which the adiabatic states $|\alpha\rangle$ are obtained as eigenfunctions of the Hamiltonian

$$\hat{H} = \hat{H}^a + \hat{H}^s; \quad \hat{H}^s = \hat{H}^h + \hat{V} \tag{1}$$

Here, the atomic Hamiltonian $\hat{H}^a$ (including the fine structure interaction) and the HF operator $\hat{H}^h$ determine the energy structure of the diabatic (bare) states of an isolated atom, while $\hat{V} = -\mathbf{E}\hat{\mathbf{d}}$ describes the coupling of the atomic dipole moment $\hat{\mathbf{d}}$ with the laser field $\mathbf{E}$. For the sake of simplicity we shall restrict this study to considering only the coupling of atoms with linearly polarized laser fields, which allows us to treat each subset of mutually coupled HF levels with the same M as an independent multilevel system.

In Sect. II we analyze the formation of bright and dark states in a simplified system where one of the strongly coupled states contains nondegenerate HF sublevels, and we discuss the manifestation of three types of states in the AT spectrum. In Sect. III, we review the MS transformation to establish a nomenclature that shall be used in this paper. Strictly speaking, finite HF sublevel separations prevent direct application of the MS transformation for describing the adiabatic state formation. However, at strong coupling, i.e., when the Rabi frequency

Ω_S of coupling of atoms with the S-laser field exceeds the HF sublevel energy separations, the MS basis [1], which consists of bright and dark states, can be utilized as a zero-order approximation for constructing the MS adiabatic states (Sect. III A). The HF Hamiltonian $\hat{H}^h$ can then be treated as a perturbation that can lead to variations in dark-state energies (Sect. III B and Apendix A); in addition, when coupling with the S-laser field is not too strong, a selectively excited MS adiabatic state can share its population with other states. We will show that besides the usual dark states there exist also chameleon states (Sect. III C) that combine the traits of both dark and bright states. The details of expression of those states in the AT spectra and some interesting features related to excitation of complementary sets of adiabatic states from different HF sublevels of the ground state by a weak probe field are discussed in Sect. IV, followed by the discussion and conclusions in Sects. V and VI, respectively. Some mathematical details related to the described results are provided in Appendices A-C. Atomic units are used through this paper unless stated otherwise.

II. TWO TYPES OF SUPPRESSED PEAKS IN THE AUTLER-TOWNES SPECTRA

Before turning to analysis of realistic excitation schemes, it is instructive to consider two simple reference model systems. Insights obtained form such analysis will be helpful for interpretation of the AT spectra in the following sections.

A. Fading peaks of dark states

Consider a final state f consisting of six closely spaced equidistant HF sublevels $|\gamma\rangle$ that are separated by $\Delta = 1.0$ MHz due to the HF interaction (Fig. 2(a)). Both ground and intermediate levels consist of a single quantum state $|g\rangle$ and $|i\rangle$, respectively. A strong laser field S of amplitude E_S is coupled with the transition $|i\rangle \to |f\rangle$, and its detuning from the transition resonance is chosen such that in RWA the diabatic level $|i\rangle$ is located exactly in the middle of the state f sublevels (see Fig.2(b)). The RWA energy of state $|i\rangle$ is chosen to be zero. The RWA energy of state $|g\rangle$ is equal to the detuning $\Delta_P = \omega_P - \omega_{ig}$ of the weak P (probe) laser field from the $|g\rangle \to |i\rangle$ transition frequency ω_{ig}.

Initially, only the ground state is populated, such that $C_g(t=0) = 1$ and $C_{\alpha\neq g}(t=0) = 0$ for the probability amplitudes C_α ($\alpha = g, i, \gamma$, $\gamma = 1, 2, \ldots, 6$). Scanning the P-laser frequency across the $|g\rangle \to |i\rangle$ resonance results in excitation of the adiabatic states. To damp Rabi oscillations in the system we introduce weak decay rates $\Gamma_\alpha = 2\pi \cdot 0.2$ MHz for all excited levels $\alpha \neq g$. The value of the P-laser Rabi frequency $\Omega_P = 10$kHz is chosen small such that optical pumping is negligible within the characteristic observation time $\tau \sim 1/\Gamma_\alpha$ [23], which implies

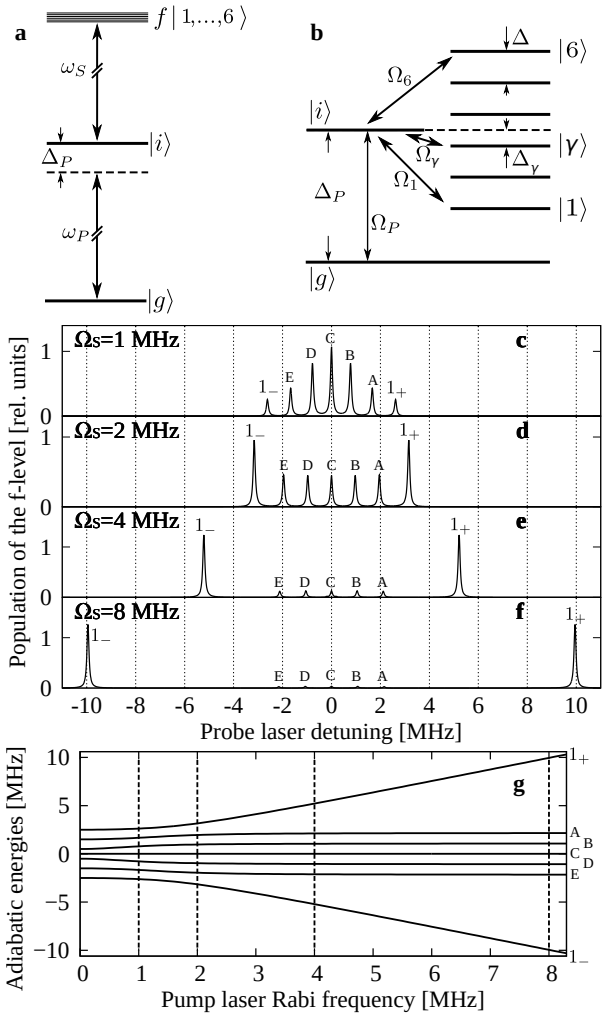

FIG. 2. (a) A model system where the ground $|g\rangle$ and intermediate $|i\rangle$ levels are coupled by a weak probe field P of frequency ω_P, while the intermediate level $|i\rangle$ is coupled by a strong laser field S to the final state f which consists of six closely spaced sublevels $|\gamma\rangle$. (b) Linkage diagram of the diabatic states in RWA. The energy of state $|i\rangle$ is chosen to be zero (dashed line). (c)-(f) Population n_f (for convenience of presentation of y-axis, units of $6 \cdot 10^{-7}$ are used) of the state f as a function of P-field detuning Δ_P at four values of the strong field Rabi frequency Ω_S. (g) Variation of adiabatic state energies with Ω_S. The upper (1_+) and lower (1_-) curves result from coupling between the intermediate state $|i\rangle$ and the bright state $|Br\rangle$ (see Fig. 5). The remaining five curves A-E correspond to dark states. The dashed vertical lines indicate the Ω_S values corresponding to the AT spectra presented in frames (c)-(f).

$C_g(t) \simeq 1$. The Rabi frequencies $\Omega_\gamma = \langle i|E_S\hat{d}|f_\gamma\rangle$ of all transitions between the intermediate $|i\rangle$ and the final states $|f_\gamma\rangle$ due to coupling with the S-laser field are assumed to be equal to Ω_S.

We solve the Schrödinger equation in RWA for an open level system and P-laser field that is too weak to cause any notable population loss due to optical pumping to

other states:

$$\frac{d}{dt}C_\alpha = -i(\Delta_\alpha - i\Gamma_\alpha/2)C_\alpha - i\sum_\beta V_{\alpha\beta}C_\beta, \qquad (2)$$

which determines the dynamics of the probability amplitudes C_α. Given the above assumptions, the only nonzero elements of the Hermitian coupling matrix V are $V_{gi} = V_{ig}^* = \Omega_P/2$, $V_{i\gamma} = V_{\gamma i}^* = \Omega_S/2$. The intensity I_f of the fluorescence emitted from the state f is proportional to its total population, which in turn is expressed via the probability amplitudes $n_f = \sum_\gamma |C_\gamma|^2$. For the sake of convenience of calculations, we assume the following form of switching of the P-field Rabi frequency:

$$\Omega_P(t) = \Omega_0(1 - \exp(-t/\tau_s)), \qquad (3)$$

where $\Omega_0 = 10\,\mathrm{kHz}$ and the switching time $\tau_s = 1/\Gamma_\alpha$. The solutions $C_\alpha(t)$ of (2) reach their quasi-stationary values at time $t \sim \tau_s$.

The values of n_f at $t = 10\tau_s$ as a function of the probe field detuning Δ_P, which are proportional to the AT spectrum $I_f(\Delta_P)$, are plotted in Fig.2(c-f) for four different values of the S-field Rabi frequency Ω_S. Increasing Ω_S to values larger than the HF separation between the adjacent states $|\gamma\rangle$ leads to a gradual decrease of intensity (Fig.2(c-e)) and eventually elimination (Fig.2(f)) of all the AT peaks except two outermost components. The latter two are associated with the excitation of adiabatic states $1_\pm$ (see Fig.2(g)), while the frequencies of the fading peaks are determined by the energies of curves $A - E$. An important feature of the suppressed ("dark") AT components is their almost unchanged frequencies (equivalent to almost constant energies of curves $A - E$), this is the typical signature of the formation of dark states that become inaccessible for excitation by the P-laser field at Ω_S exceeding Δ. In contrast, the surviving pair of ("bright") peaks $1_\pm$ increases its frequency separation with increasing Ω_S, and it is always available for excitation by the P-laser field (see details in Sec. III B).

B. Peaks associated with the chameleon states

The second reference atomic configuration consists of five levels presented in Fig.3(a) which mimics a realistic situation akin to the ladder scheme of Fig.1(b) with $M = 1$ (see Sect. V for detail). The upper sublevels $|f\rangle_2$, $|f_0\rangle$ (equivalent to the $|f\rangle_2$ and $|f_{\chi=0}\rangle$ sublevels of state f in Fig.1(b)) have only negligible HF interaction which is disregarded. The intermediate sublevels $|i\rangle_2$, $|i_0\rangle$ (equivalent to $|i\rangle_2$ and $|i_{\chi=0}\rangle$ states in Fig.1(b)) have the energy splitting $\Delta\varepsilon_{20}$ of 30 MHz and are mixed by the HF interaction with frequency $\varpi_I = 50\,\mathrm{MHz}$ (see App. C). The strong S-laser field couples the states i and f as shown in Fig.3(b) with slightly different Rabi frequencies $\Omega_{S_2} = \Omega_S$ and $\Omega_{S_0} = \Omega_S/\sqrt{1.5}$ (see App. B after Eq.(B3)). The RWA energies of sublevels $|f\rangle_2$, $|f_0\rangle$ are chosen to be zero. The detuning of the S-field frequency is such that the RWA energies of the intermediate sublevels are $\Delta_{i_2} = 50\,\mathrm{MHz}$ and $\Delta_{i_0} = 20\,\mathrm{MHz}$. The RWA energy of state $|g\rangle$ is given by the P-field detuning Δ_P from the two-photon resonance (see Fig. 3(a)).

The weak P-field probes the resulting adiabatic states from the ground state $|g\rangle$ via a single allowed optical

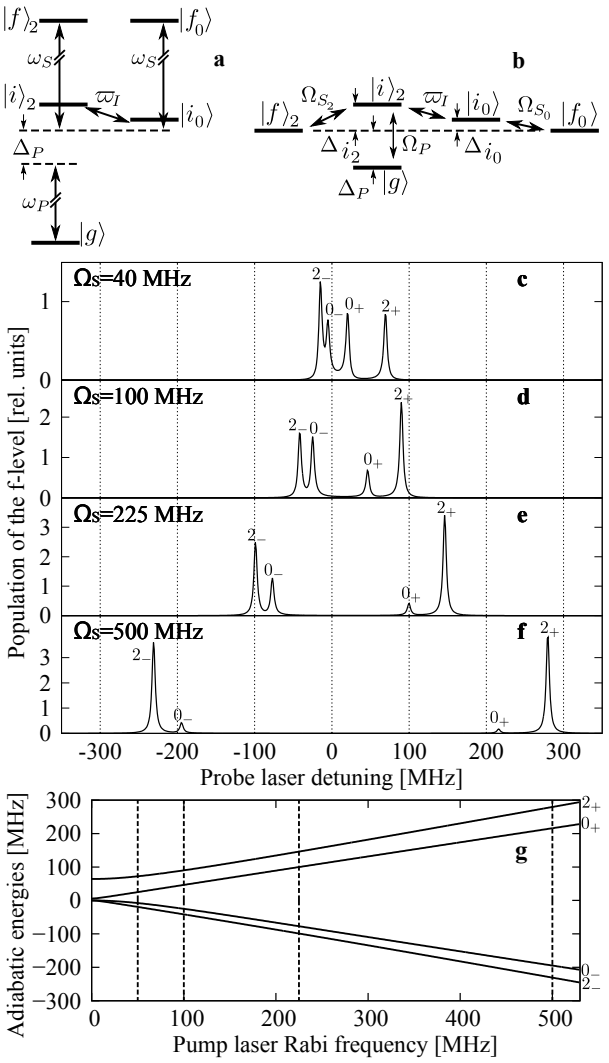

FIG. 3. (a) Ladder-like excitation scheme where the ground state $|g\rangle$ and component $|i\rangle_2$ of the intermediate state i are coupled by a weak probe field P, while state i is in turn coupled by a strong laser field S to the final two-component degenerate state f. (b) Linkage diagram for RWA states. The energies of levels $|f\rangle_2$, $|f_0\rangle$ are chosen to be zero (dashed line). (c)-(f) Population n_f (for convenience of presentation of y-axis, units of $5\cdot10^{-9}$ are used) of state f as a function of P-field detuning Δ_P at four different values of Ω_S. (g) Energies of adiabatic states as a function of Ω_S. The diverging pairs of states $2_\pm, 0_\pm$ result from coupling of levels $|f\rangle_2, |i\rangle_2$ and $|f_0\rangle, |i_0\rangle$ by the S-laser field as depicted in frame (b). The dashed vertical lines correspond to the values of Ω_S used to obtain frames (c)-(f).

transition $|g\rangle \rightarrow |i\rangle_2$. The observed fluorescence signal is proportional to the total steady-state population n_f of state f. This population can be found via asymptotic solution of the Schrödinger equation (2) upon adiabatic switching (3) of the P-field Rabi frequency. At $t = 0$ the entire population is in state g. The chosen amplitude $\Omega_0 = 0.1\,\mathrm{MHz}$ is too small to cause any notable depletion of state g due to optical pumping [23–25]. The relaxation rates $\Gamma_\alpha = 1/\tau_\alpha$ for the upper and intermediate levels are calculated using the values $\tau_f = 52.4$ns and $\tau_i = 16.3$ns that correspond to the radiative lifetimes of the $4d_{5/2}$ and $3p_{3/2}$ states of Na, respectively [26, 27].

The dependence of the population $n_f(t = 10\tau_s)$ on the probe field detuning Δ_P is shown in Fig.3(c-f). The usual "dark" AT peaks are no longer seen; instead, one observes two pairs of diverging peaks. Two of them, $2_\pm$, evidently form a "bright" pair with more or less similar amplitudes for all considered values of Ω_S. The other pair, $0_\pm$, reveals a disguising behavior: on one hand the separation between the two components increases with increasing Ω_S, which is a trait typical of bright states; on the other hand, the two peaks lose their intensity and eventually vanish at very large Ω_S similarly to the dark states in the example of Sect. II A. For this disguising nature we term the corresponding states the "chameleon" states, meaning states that combine the properties of both bright and dark states and change the way those properties are exhibited in the excitation spectrum depending on the coupling field strength. The occurrence of dark and chameleon states will be analyzed in more detail in the following sections.

III. ADIABATIC STATES' APPROACH

Manipulation of quantum states by coherent laser fields is usually associated with large interaction Rabi frequencies. Under such conditions it is often possible to treat the HF interaction operator $\hat{H}^h$ (1) as a perturbation of the laser-atom interaction $\hat{V}$, such that in first approximation the adiabatic states can be represented by eigenvectors of the simplistic operator $\hat{H}^a + \hat{V}$. The operator $\hat{V}$ couples two states, A and B, each consisting of N_A and N_B degenerate sublevels, respectively (see Fig.4(a)). In RWA, the energy separation Δ_S between states A and B is given by the detuning of the strong coupling field. We assume that $N_A \geq N_B$. In the case of the excitation scheme shown in Fig.2(a) $N_A = 6$ (state f) and $N_B = 1$ (state i), while in the scheme of Fig.3(a) $N_A = 2$ (state f) and $N_B = 2$ (state i).

A. Morris-Shore (MS) transformation

The problem of diagonalizing the operator $\hat{H}^a + \hat{V}$ for a degenerate two-level systems was first solved by J.R. Morris and B.W. Shore [1]. We shall briefly reproduce their results here in order to introduce the notations used in the following sections. It is convenient to operate with subspaces Λ_A and Λ_B of diabatic (bare) state vectors $|a_\gamma\rangle$ and $|b_\chi\rangle$ of states A and B (see Fig.4(a)). The operator for coupling with the S-laser field, $\hat{V}$, projects the subspace Λ_B onto the subspace Λ_A and vice versa:

$$\hat{V}\Lambda_B \rightarrow \Lambda_A; \quad \hat{V}^\dagger\Lambda_A \rightarrow \Lambda_B. \tag{4}$$

The idea of the MS transformation lies in the reduction of the general excitation linkage pattern in the basis $\{|b_\chi\rangle, |a_\gamma\rangle\}$ (Fig.4(a)) to a new scheme in MS basis consisting of coupled pairs of states ($|\beta_\chi\rangle$ in Λ_B and $|\alpha_\chi\rangle$ in Λ_A) and uncoupled single states, as shown in Fig.4(b).

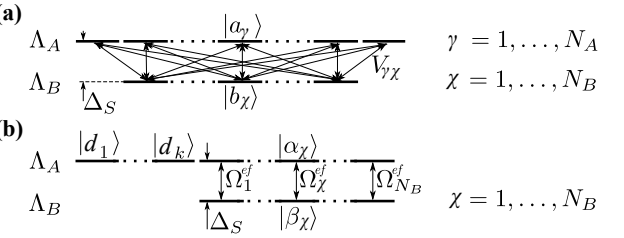

FIG. 4. (a) RWA linkage pattern for laser coupling of degenerate systems Λ_A and Λ_B (general case); (b) the same after performing the Morris-Shore transformation [1].

An important feature of the MS basis is the conservation of orthogonality (see also Fig.4(b)): images of any pair of mutually orthogonal states $|\beta\rangle, |\beta'\rangle$ from Λ_B in Λ_A, $|\alpha\rangle = \hat{V}|\beta\rangle$ and $|\alpha'\rangle = \hat{V}|\beta'\rangle$, preserve the mutual orthogonality:

$$\langle\alpha'|\alpha\rangle = \langle\beta'|\hat{V}^\dagger\hat{V}|\beta\rangle = 0. \tag{5}$$

This is only possible if all states $|\beta_\chi\rangle$ are eigenvectors of the positive Hermitian operator $\hat{V}^\dagger\hat{V}$ acting in the subspace Λ_B [1]:

$$\hat{V}^\dagger\hat{V}|\beta_\chi\rangle = \frac{1}{4}\left|\Omega_\chi^{ef}\right|^2|\beta_\chi\rangle; \quad |\alpha_\chi\rangle = 2/|\Omega_\chi^{ef}| \cdot \hat{V}|\beta_\chi\rangle. \tag{6}$$

The normalized states $|\alpha_\chi\rangle$ that are coupled with states $|\beta_\chi\rangle$ with MS effective Rabi frequencies Ω_χ^{ef} ($\chi = 1, 2...N_B$) are found as their images according to Eq. (6) and represent a set of N_B bright states [1]. The remaining $\kappa = N_A - N_B$ state vectors $|d_1\rangle, ..., |d_\kappa\rangle$ in the subspace Λ_A, which are chosen to be orthogonal to all the bright states $|\alpha_\chi\rangle$, are dark states because they are decoupled from the interaction with the laser field.

Among the $N_A + N_B$ possible spectral lines in the AT spectrum one can therefore identify $N_A - N_B$ peaks corresponding to dark states, provided that the relatively weak HF interaction that enables their excitation by the probe laser field has been taken into account (see Sec. III B). Note, that some values of Ω_χ^{ef} in Eq. (6) may happen to be zero, in which case the number of states appearing as "dark" peaks exceeds the expected value of $N_A - N_B$.

B. Properties of the dark states and the effect of HF interaction.

The MS formalism enables finding the full set of adiabatic states for the linkage diagram depicted in Fig. 2(b) in the limit of large Rabi frequencies $\Omega_\gamma > \Delta_\gamma$. To clarify the properties of dark states, we shall consider the general case of Fig. 5(a) where state i has a single level $|i\rangle$ that is coupled to N_A HF levels $|\gamma\rangle$ of state f. The coupling strengths between level $|i\rangle$ from subspace Λ_B and levels $|\gamma\rangle$ from subspace Λ_A are given by the respective Rabi frequencies Ω_γ,

$$\Omega_\gamma = 2\langle i|\hat{V}|\gamma\rangle; \quad \hat{V} = \frac{1}{2}\sum_\gamma \Omega_\gamma |\gamma\rangle\langle i| + h.c. \qquad (7)$$

In what follows we shall consider the space $\Lambda = \Lambda_A \oplus \Lambda_B$ that contains a complete set of $N_A + 1$ diabatic vectors $\{|\xi\rangle\}$ ($\xi = i, 1, \ldots, N_A$). In the basis of $|\xi\rangle$ the HF operator $\hat{H}^h$ (1) is a $N_A + 1$-dimensional diagonal matrix that contains the RWA energies Δ_ξ of states $|\xi\rangle$. With the RWA energy of level $|i\rangle$ chosen as zero reference (dashed line in Fig. 5), one can write

$$\hat{H}^h = \sum_\gamma \Delta_\gamma |\gamma\rangle\langle\gamma|; \quad \Delta_\gamma = \omega_{\gamma i} - \omega_S. \qquad (8)$$

Here, $\omega_{\gamma i}$ are frequencies of the atomic transitions $|i\rangle \to |\gamma\rangle$ and ω_S is the S-laser frequency.

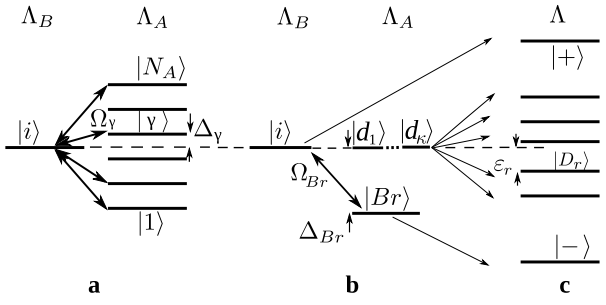

FIG. 5. (a) Diabatic state coupling diagram in RWA corresponding to the excitation scheme of Fig.2. The single level $|i\rangle$ (state i in Λ_B) is coupled to a set of levels $|\gamma\rangle$ ($\gamma = 1, 2, \ldots, N_A$) (state f in Λ_A) by the S-laser field. The energy of level $|i\rangle$ is chosen as zero energy reference. (b) Coupling diagram for dark and bright states in the MS basis $\Im_{MS}$ disregarding the HF splitting. The energy shift Δ_{Br} of the bright state is determined by Eq.(11). (c) Energies of the adiabatic states. The coupling (10) between level $|i\rangle$ and the bright state $|Br\rangle$ leads to the formation of the adiabatic states $|+\rangle, |-\rangle$, the energies of which diverge with increasing coupling strength according to Eq. (13). The energy shifts ε_r of the $\kappa = (N_A - 1)$ dark states and their mixing with the bright states $|+\rangle, |-\rangle$ occur because of the HF interaction operator H^h.

At strong coupling with the S-laser field, such that $\hat{V}$ becomes the dominant part of $\hat{H}^s$ in Eq. (1), the adiabatic states are obtained in the zero-order approximation as eigenstates of $\hat{V}$, whereby $\hat{H}^h$ is disregarded and the HF splitting is assumed to be $\Delta_\gamma = 0$ (see Fig.5(b)). The MS transformation then yields a simple structure of bright and dark states. The operator $\hat{V}^\dagger\hat{V}$ (6) is one-dimensional ($\chi = 1$) and has a single eigenstate $|\beta_{\chi=1}\rangle = |i\rangle$. The single bright state is an image (6) of level $|i\rangle$:

$$|Br\rangle \equiv |\alpha_{\chi=1}\rangle = 2\hat{V}|i\rangle/|\Omega_{Br}| = \frac{1}{|\Omega_{Br}|}\sum_\gamma \Omega_\gamma |\gamma\rangle, \qquad (9)$$

where we have used the representation (7) for the coupling operator $\hat{V}$. The normalization factor Ω_{Br} is equal to the effective MS Rabi frequency $\Omega^{ef}_{\chi=1}$ (7):

$$\Omega^2_{Br} = 4\langle i|\hat{V}^\dagger\hat{V}|i\rangle = \sum_\gamma |\Omega_\gamma|^2. \qquad (10)$$

The $\kappa = N_A - 1$ mutually orthogonal dark states $|d_r\rangle$ of the subspace Λ_A can be arbitrarily assigned to the "dark" subspace Λ^D that is orthogonal to the bright state $|Br\rangle$. Together, these states define the MS basis $\Im_{MS} = \{|i\rangle, |Br\rangle, |d_r\rangle\}$ ($r = 1, ..., N_A - 1$) with linkage pattern as depicted in Fig.5(b). It is convenient to choose the two coupled orthogonal states $\{|i\rangle, |Br\rangle\}$ as basis vectors of the 2-dimensional subspace $\Lambda^\pm$.

A quantitative study of the effect of HF interaction on the dark states is given in Appendix A. Here, we summarize results obtained in the case of strong coupling ($\Omega_{Br} \gg \Delta_\gamma$). Treatment of the HF operator $\hat{H}^h$ (8) as a perturbation has a twofold effect: (i) in addition to the energy shift of the bright state,

$$\Delta_{Br} = \langle Br|\hat{H}^h|Br\rangle = \frac{1}{\Omega^2_{Br}}\sum_\gamma |\Omega_\gamma|^2 \Delta_\gamma, \qquad (11)$$

a splitting of energies of the dark states $|d_r\rangle$ is also observed (see Fig.5(b)-(c)); (ii) the action of the HF operator $\hat{H}^h$ leads to population sharing within the system of all zero-order adiabatic states, which is caused by the off-diagonal matrix elements of $\hat{H}^h$ between the bright and dark states [16, 28]. This twofold effect is formally captured by the representation (A4) of the aggregate Hamiltonian $\hat{H}^s = \hat{H}_{MS} + \hat{H}_{\pm D} + \hat{H}_{D\pm}$.

The operator $\hat{H}_{MS}$ (A5) acts independently in the subspaces of coupled $\Lambda^\pm$ and dark Λ^D states without mixing their vectors. In the strong interaction limit $\Omega_{Br} \gg \Delta_\gamma$ the diagonalization of $\hat{H}_{MS}$ results in the construction of two zero-order sets of adiabatic states (see Fig.5(c)). The first set consists of two bright adiabatic states

$$\begin{aligned} |+\rangle &= \cos\theta|i\rangle + \sin\theta|Br\rangle; \\ |-\rangle &= -\sin\theta|i\rangle + \cos\theta|Br\rangle, \end{aligned} \qquad (12)$$

which are linear combinations [16] of the coupled vectors $|i\rangle, |Br\rangle$. The respective adiabatic state energies $\varepsilon_\pm$ are

$$\hat{H}_{MS}|\pm\rangle = \varepsilon_\pm|\pm\rangle;\ \varepsilon_\pm = \frac{1}{2}\left[\Delta_{Br} \pm \sqrt{\Delta_{Br}^2 + \Omega_{Br}^2}\right], \tag{13}$$

while the mixing angle $\theta = \arctan(-\Omega_{Br}/\Delta_{Br})$ provides a measure of amplitudes sharing between the bright diabatic vectors $|i\rangle, |Br\rangle$. The other set includes $N_A - 1$ adiabatic "dark" states $|D_r\rangle$ that are eigenstates of the operator $\hat{H}_{MS}$ in subspace Λ^D. Their energies ε_r exhibit a small offset [6] from the initial energies Δ_γ of the diabatic (bare) states:

$$\Delta_r < \varepsilon_r < \Delta_{r+1}, \quad r = 1, 2, \ldots, N_A - 1. \tag{14}$$

The operators $\hat{H}_{\pm D}, \hat{H}_{D\pm}$ (A6) act between the subspaces $\Lambda^\pm$ and Λ^D, leading to mixing between the bright and dark states. Strong coupling ($\Omega_{Br} \gg |\Delta_\gamma|$) is equivalent to a large energy separation ($\sim \Omega_{Br}$) of the adiabatic states $|+\rangle, |-\rangle$ from all dark states. For this reason, the probability $P_\pm$ to find the MS bright vectors $|i\rangle, |Br\rangle$ in the perturbed dark adiabatic basis $|D_r\rangle$, which is associated with the energy curves A-E in Fig.2(g), does not exceed the ratio R ([29], Chapter VI)

$$P_\pm \leqslant R = \max\left(|\Delta_\gamma|\right)^2 / \Omega_{Br}^2. \tag{15}$$

This is reflected in the AT spectra shown in Fig.2((c)-(f)): when a weak probe laser field excites the adiabatic states, the ratio between the intensities of "dark" and "bright" peaks (proportional to $P_\pm$) decreases as Ω_{Br}^{-2} with increasing Ω_{Br}. We emphasize here the role played by the HF interaction: despite the dark states being entirely decoupled from interaction with the S-laser field, they can nevertheless be excited due to mixing induced by the HF interaction with the bright states. For this reason, at moderate S-laser intensities ($\Omega_{Br} \simeq |\Delta_\gamma|$) the dark states should rather be considered as kind of "grey" states that appear in the AT spectrum as almost stationary peaks (i.e. peaks that do not change energy upon variation of Ω_{Br}, see Fig.2(c),(d)) and disappear from the spectrum (see Fig.2(e),(f)) at large Rabi frequencies ($\Omega_{Br} \gg |\Delta_\gamma|$).

C. Properties of "chameleon" states and the effect of HF interaction

Quantitative analysis of the spectra shown in Fig.3, and in particular the behavior of peaks $0_\pm$ associated with excitation of the chameleon states, can be performed similarly to that presented above for the dark states. It makes use of either the projection operators' technique discussed in Appendix A or the analytical methods developed in [30]. Here, we shall only provide a brief semi-quantitative description.

In the limit of strong coupling ($\Omega_S \gg \varpi_I, \Delta_{i_{0,2}}$), the interaction associated with the HF operator (see Fig.3(b) for notations)

$$\hat{H}^h = (\varpi_I |i\rangle_2\langle i_0| + hc) + \Delta_{i_0}|i_0\rangle\langle i_0| + \Delta_{i_2}|i\rangle_2\langle i|_2 \tag{16}$$

can be disregarded. The two pairs of coupled vectors $|i\rangle_2, |f\rangle_2$ and $|i_0\rangle, |f_0\rangle$ are independent. A strong interaction with the S-laser field (mixing angle $\theta \simeq \pi/4$) gives rise to two pairs of adiabatic states (12): $|2_\pm\rangle = (|f\rangle_2 \pm |i\rangle_2)/\sqrt{2}$ and $|0_\pm\rangle = (|f_0\rangle \pm |i_0\rangle)/\sqrt{2}$. The energies of those states vary with Ω_S as $\varepsilon_{2_\pm} = \pm\Omega_{S_2}/2$ and $\varepsilon_{0_\pm} = \pm\Omega_{S_0}/2$, respectively (see Eq. (13)). The energy separations $\Delta_{20_+} = \varepsilon_{2_+} - \varepsilon_{0_+}$ and $\Delta_{02_-} = \varepsilon_{0_-} - \varepsilon_{2_-}$ between the adjacent states from different pairs grow as $\Delta_S \simeq (\Omega_{S_2} - \Omega_{S_0})/2 = \Omega_S/(6 + 2\sqrt{6})$ with increasing Ω_S. At the same time, the mixing frequencies $\varpi_\pm = \langle 0_\pm|\hat{H}^h|2_\pm\rangle = \varpi_I/2$ introduced by the operator (16) remain constant, and in accordance with Eq. (15) one should expect the intensities of the $0_\pm$ peaks to decrease with Ω_S as $\varpi_\pm^2/\Delta_S^2$.

We note two circumstances: (i) the off-diagonal elements $\langle 0_+|\hat{H}^h|2_-\rangle = \varpi_I/2$ that lead to state mixing can be dropped because of the large energy separation ($\simeq \Omega_S$) between states $|0_+\rangle, |2_-\rangle$; (ii) the diagonal elements of the operator $\hat{H}^h$ give rise to energy shifts $\delta\varepsilon$ of the adiabatic states: $\delta\varepsilon_{2_\pm} = \Delta_{i_2}/2$, $\delta\varepsilon_{0_\pm} = \Delta_{i_0}/2$. Hence, the energies of the adiabatic states shift linearly upon variation of Ω_S,

$$\varepsilon_{2_\pm} = \Delta_{i_2}/2 \pm \Omega_S/2; \quad \varepsilon_{0_\pm} = \Delta_{i_0}/2 \pm \Omega_S/\sqrt{6}, \tag{17}$$

and the separations $\Delta_{20_+}, \Delta_{02_-}$ between the adjacent states also increase linearly with Ω_S (see Fig.3(g)). The role of the HF interaction here is that of mixing $|2_+\rangle$ into $|0_+\rangle$, and $|2_-\rangle$ into $|0_-\rangle$. The fraction $P_\pm$ of this admixture is given by ([29])

$$P_+ = \varpi_I^2/\Delta_{20_+}^2; \quad P_- = \varpi_I^2/\Delta_{02_-}^2. \tag{18}$$

Without the HF interaction, the excitation of both adiabatic states $|0_\pm\rangle$ by the P-laser field is forbidden due to absence of their optical coupling with the ground state $|g\rangle$ (see Fig.3(a,b)). The HF mixing introduces a notable admixture of $|i_2\rangle$ in the composition of $|0_\pm\rangle$, consequently leading to observation of the $0_\pm$ components in the AT spectrum. As Ω_S is further increased, the mixing coefficients $P_\pm$ decrease as Ω_S^{-2} and the chameleon states gradually disappear from the AT spectrum.

IV. REAL ATOMIC SYSTEMS

Having explained the effect of HF interaction on the formation of adiabatic states and on their populations

in the case of simplified model systems shown in Figs. 2 and 3, we shall now analyze an example of a real HF level system in Na atoms. We consider the three-level ladder excitation scheme depicted in Fig. 1(a). The detunings $\Delta_S = \omega_S - \omega_{4d,3p(F'=2)}$ and $\Delta_P = \omega_p - \omega_{3p(F'=2),3s(F'')}$ of the coupling (S) and probe (P) laser fields are defined relative to the resonance frequencies of the respective HF transitions.

A. Numerical calculations

To simulate the AT spectra, we solve numerically the optical Bloch equations (OBEs) for the density matrix [31]:

$$\frac{d\rho}{dt} = -i\left[\hat{H}\rho\right] + \hat{R}\rho. \tag{19}$$

Here, the total Hamiltonian $\hat{H}$ of the atom-laser system includes the atomic-structure Hamiltonian $\hat{H}^a + \hat{H}^h$ and the dipole operators $\hat{V}_{P,S} = -\hat{\boldsymbol{d}}\boldsymbol{E}_{P,S}$ defining the interaction of atoms with the P- and S-laser fields. The term $\hat{R}$ accounts for the relaxation and population transfer processes due to the spontaneous emission and for the finite laser linewidths. Equation (19) can be decomposed into a system of OBEs for the diagonal density matrix elements $\rho_{\alpha_k\alpha_j}$ ($\alpha = g, i, f$), also called Zeeman coherences, and for the off-diagonal elements $\rho_{\alpha_k\beta_j}$ ($\alpha \neq \beta$), also termed optical coherences. The indices g_k, i_k and f_k run over all the HF and Zeeman sublevels of the ground, intermediate and final states, respectively. The solution of this system of equations can be readily obtained numerically by applying the Split Operator Technique [32–34].

Each laser (of amplitude $E_{P,S}$ and both linearly polarized along the quantization axis z) stimulates a variety of transitions among the HF and Zeeman sublevels. It is convenient to describe the laser induced couplings using the characteristic Rabi frequencies $\Omega_{P,S}$ that drive the transitions $3s-3p$ and $3p-4d$ [23]:

$$\Omega_P = E_P|\langle 3s \parallel D \parallel 3p\rangle|; \quad \Omega_S = E_S|\langle 4d \parallel D \parallel 3p\rangle| \tag{20}$$

Here, the transitions are considered unresolved with respect to fine and hyperfine structure, and $\langle nL||D||n'L'\rangle$ is the corresponding reduced matrix element [35]. The principal quantum numbers and the orbital, electronic and total angular momenta are denoted by n, L, J, and F, respectively. Rabi frequencies of individual fine $\{LJ \rightarrow L'J'\}$ and HF $\{LJF \rightarrow L'J'F'\}$ transitions are then defined by the tabulated line strength values [35]. The Rabi frequencies for individual transitions $\{LJFM \rightarrow L'J'F'M\}$ between Zeeman sublevels M in the case of linearly polarized excitation are obtained using the formulae provided in [35, 36], and the respective values can be found in [23, 24].

The calculations are performed for the conditions of the experiment described in [37]: a supersonic beam of sodium atoms with the mean flow velocity of 1160 m/s is crossed by two counterpropagating laser beams at right angles. Both laser beams are linearly polarized in the same direction that is perpendicular to the atomic beam axis, which implies the selection rule $\Delta M = 0$ for the magnetic quantum numbers. The intensity distribution in the laser beams corresponds to Gaussian switching of Rabi frequencies $\Omega_{P,S}(t) = \Omega_{P,S}\exp(-2t^2/\tau^2_{P,S})$. The calculation yields the total number N_f of photons emitted by a single atom in the $4d_{5/2}$ state upon crossing the laser-atom interaction zone. Laser beam waists are chosen such that the transit times of atoms through the P- and S-laser beams are $\tau_P = 350ns$ and $\tau_S = 1050ns$. The laser linewidths are assumed to be 1 MHz.

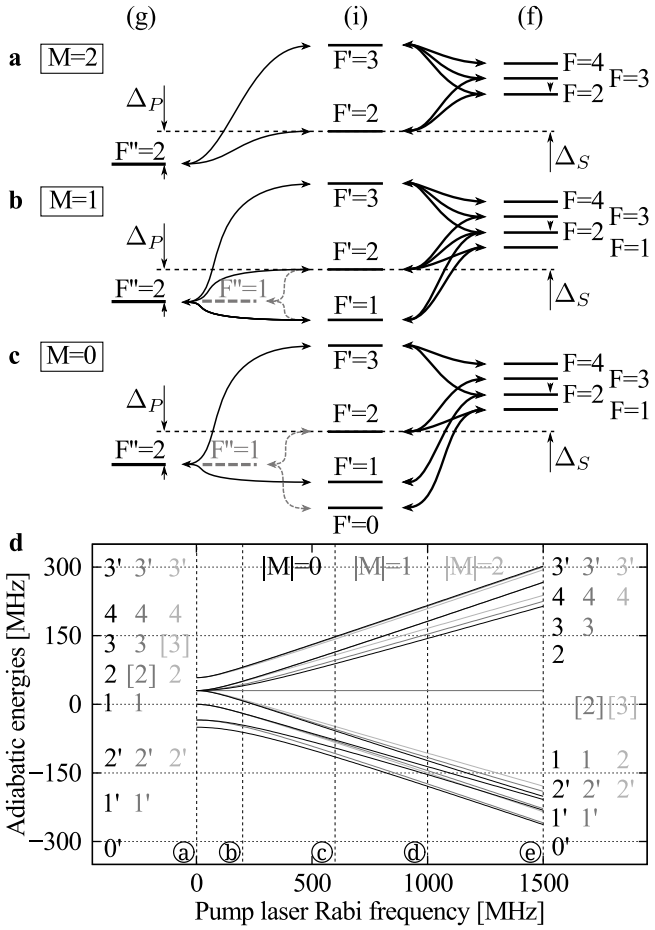

FIG. 6. Coupling patterns in RWA for the $3s_{1/2}(F'' = 1, 2; M) \rightarrow 3p_{3/2}(F'; M) \rightarrow 4d_{5/2}(F; M)$ excitation at the pump laser detuning $\Delta_S = -30$ MHz for Zeeman sequences with (a) $M = 2$; (b) $M = 1$; (c) $M = 0$. The horizontal dashed line shows the zero-energy reference that is set equal to the energy of $3p_{3/2}(F' = 2)$. Energies of the $4d_{5/2}$ HF levels are indistinguishable; they are drawn resolved only to show their linkages with the $3p_{3/2}$ state HF levels. (d) Energies ε_a of the adiabatic states vs pump field Rabi frequency Ω_S. The dashed vertical lines correspond to the Ω_S values presented in Fig. 7, frames (a)-(e). The square brackets indicate states which evolve into dark states.

B. Results for the excitation scheme of Fig.1(a)

Figure 6(a) – (c) shows the possible couplings between the HF sublevels upon excitation of the $3p_{3/2} \rightarrow 4d_{5/2}$ transition by linearly polarized light. Since only the transitions with $\Delta M = 0$ are allowed, and the P-laser field is weak such that it does not induce any notable optical pumping, we consider the manifolds with $M = 0, 1$ and 2 separately. Figure 7 shows the AT spectra, calculated as the total flux of photons N_f emitted by the $4d_{5/2}$ state for five different values of the S-field Rabi frequency Ω_S. Simulations are performed using the parameters $\Omega_P = 1\,\mathrm{MHz}$ and $\Delta_S = -30\,\mathrm{MHz}$. Figure 6(d) also shows the calculated adiabatic state energies as a function of Ω_S; those energies are used in Figs. 7,8 to indicate the expected positions (dashed lines) of the AT peaks. Individual adiabatic states are labeled according to the quantum numbers F, M of the diabatic (bare) states in the limit of $\Omega_S = 0$ (see Fig.6(d)). The numbers denote the HF quantum numbers in the $4d_{5/2}$ state, while the numbers with a prime correspond to the HF quantum numbers in the $3p_{3/2}$ state. Zeeman quantum numbers M in Figs. 6 and 7 are indicated by colour: $|M| = 0$ in black, $|M| = 1$ in gray and $|M| = 2$ in light gray. Because of the mirror symmetry σ_z of the system relative to any plane containing the quantization axis z, the adiabatic state energies do not depend on the sign of M [29, 35].

At very low Ω_S (Fig.7(a)), the excitation spectrum exhibits a strong peak at $\Delta_P = 30\,\mathrm{MHz}$ that corresponds to two-photon excitation of the $4d_{5/2}$ state, and three much weaker peaks of $\Delta_P = 59$, 0, $-34\,\mathrm{MHz}$ that occur because of the one-photon excitation of levels $F' = 1, 2$ and 3 of the $3p_{3/2}$ state by the P-laser field. As Ω_S is increased (Fig.7(b)-(e)), the creation of adiabatic states and their gradual conversion into pairs of states with diverging energies and into dark states with unchanging energies is observed in Fig.6(d). An adiabatic state can be considered a dark state (see the corresponding discussion in Sec III B) when its energy no longer changes with increasing Ω_S (curves [2],[3] in Fig.6(d)). In contrast, the bright pairs $|\alpha_\chi\rangle, |\beta_\chi\rangle$ of Morris-Shore states (see Fig.4(b)) would typically form adiabatic pairs $|\pm\rangle$ (12), the energy separation between which steadily increases with increasing Ω_S (see, e.g., the peaks $1_\pm$ in Fig. 2(g), or $0_\pm$ and $2_\pm$ in Fig. 3(g)).

At large Ω_S the dependence of adiabatic state energies ε_a on Ω_S is linear (see also Eq. (17)):

$$\varepsilon_a = \Pi_a \Omega_S + e_a, \tag{21}$$

where the slope coefficient $\Pi_a = \Omega^{ef}_{\chi=a}/\Omega_S$ is determined by the effective MS Rabi frequency of a given adiabatic state on Fig.6 and e_a is the respective energy determined by the HF operator $\hat{V}^h$. For a dark state, the coefficient $\Pi_D = 0$, while for any pair of $|+\rangle$ and $|-\rangle$ states the relation $\Pi_{a_+} = -\Pi_{a_-}$ is valid. The adiabatic states from different diverging pairs, that have identical slope

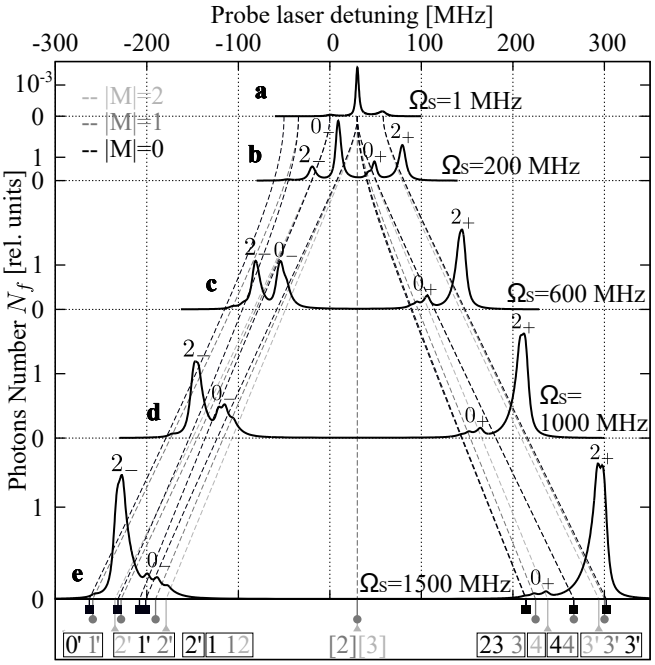

FIG. 7. The total number of photons N_f (in units of $2 \cdot 10^{-3}$) emitted by $4d_{5/2}$ state vs P-field detuning for the $3s_{1/2}(F'') \rightarrow 3p_{3/2} \rightarrow 4d_{5/2}$ excitation sequences with $F'' = 2$. We assume a uniform population distribution over the Zeeman components M of the $3s_{1/2}$ state HF level $F'' = 2$. The Λ-type dashed lines show the expected positions of the AT peaks: the black squares label energies of the adiabatic states with $M = 0$, the gray circles – with $|M| = 1$ and the light gray triangles – with $|M| = 2$. If several expected lines partially merge and form a complex multiplet at $\Omega_S = 1500\,\mathrm{MHz}$, the respective label numbers are boxed in the same rectangle. Numbers in the boxes refer to the same indices as those used for labeling the adiabatic states in Fig.6(d).

coefficients $\Pi_{a_\pm}$, may partially merge at large Ω_S, forming complex "bright" multiplets in the AT spectrum (see Fig.7(d)). It is convenient to label the components of those multiplets by the corresponding indexes $a_\pm$. In the case of Figs. 6(d) and 7, two different values $\Pi_{2_+,0_+}$ are seen with the ratio $\Pi_{2_+}/\Pi_{0_+} = \sqrt{1.5}$ (see text after Eq.(B3) in App. B).

Note that the energies of the two dark states in Fig.6 (d) do not depend on Ω_S (curves [2], [3]). This is understandable because the negligibly small HF interaction in the $4d_{5/2}$ state implies fulfillment of the classical dark state situation as described in [1], whereby the dark states are always decoupled from interaction with the S-laser field and, hence, are not observed in the AT spectra. This circumstance is also supported by the data presented in Fig.7.

An important feature of the AT spectra in Fig.7 is the gradual fading of the initially "bright" components 0_+ and 0_- that happens alongside with the expected increase of separation between those components as Ω_S is increased. The other pair of "bright" components 2_+, 2_- shows increasing frequency shifts of both components

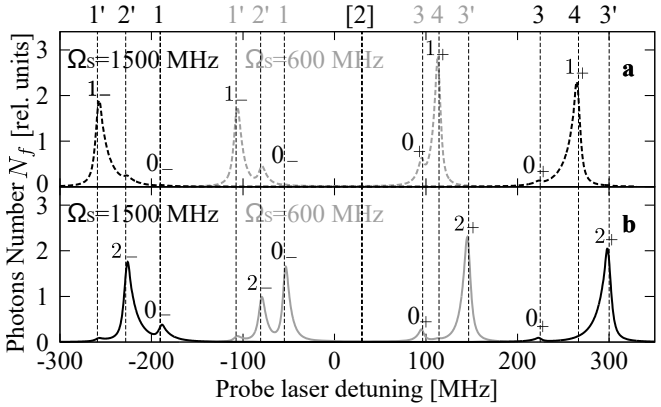

FIG. 8. Same as in Fig.7 but for $M = 1$ Zeeman sequence upon excitation by the P-laser field from (a) $F'' = 1$ (dashed lines) and (b) $F'' = 2$ (solid lines). The spectra correspond to the linkage scheme of the Fig.6(b). Each frame shows spectra for two different S-field coupling strengths: $\Omega_S = 600$ MHz (gray) and $\Omega_S = 1500$ MHz (black). The vertical dashed lines indicate the respective adiabatic state energies.

that do not vanish with increasing Ω_S, which is a classical trait of an AT doublet. This clearly demonstrates the differences in spectral behaviour of the bright (2_+, 2_-) and chameleon (0_+, 0_-) states, whereby the existence of the latter is solely due to the presence of the HF interaction.

The final interesting and, perhaps, the most practically useful feature is shown in Fig. 8. If Ω_S is sufficiently large, and the adiabatic states are probed from either $F'' = 2$ (solid lines in frame (b)) or $F'' = 1$ (dashed curves in frame (a)) of the ground state, the AT spectra exhibit two sets of peaks, $2_\pm$ and $1_\pm$, that are complementary to each other and are associated with different adiabatic states. This means that at high Ω_S the excitation by the probe field from different ground state hyperfine components leads to population of orthogonal sets of adiabatic states that correlate with different HF levels in states i and f.

V. DISCUSSION

The numerical results presented in Sect. IV can be explained by the properties of adiabatic states. As is natural to expect, the HF level linkage diagram presented in Fig.1(a) transforms into a set of independent simple 3-level blocks as shown in Fig.1(b) when hyperfine coupling is broken down by interaction with very strong laser fields ($\Omega_S \gg 110$MHz, $\Omega_P \gg 1.8$GHz) that exceed the largest HF level separations (see App. B for explanation of the basis of broken-down HF coupling). Interestingly, such architecture of quasi-independent blocks is preserved even in the HF basis when the HF coupling is only partly broken, i.e., when one can disregard the HF coupling in the intermediate state i ($3p_{3/2}$) (strong S-laser) but not in the ground state g ($3s_{1/2}$) (weak P-laser). One can show by direct calculations that all sequences of mapping of state vectors $|F''M\rangle$ from the ground to intermediate to final state by the operators $\hat{V}_P$ and $\hat{V}_S$ give raise to mutually orthogonal excitation ladders (see Appendix C)

$$\hat{V}_P|F''M\rangle \to |i\rangle_{F''M}; \quad \hat{V}_S|i\rangle_{F''M} \to |f\rangle_{F''M}, \qquad (22)$$

where $|F''M\rangle$ is the initial diabatic state vector in state g, while $|i\rangle_{F''M}$ and $|f\rangle_{F''M}$ are its images in the subspaces of states i and f following the action of the laser-atom interaction operators $\hat{V}_P$ and $\hat{V}_S$, respectively. Hence, each ladder (22) constitutes a unique and independent excitation path predefined by the choice of $F''M$. It is convenient to associate a double-index $\eta = F'', M$ with each of those paths, with excitation steps denoted as $|g\rangle_\eta, |i\rangle_\eta$, and $|f\rangle_\eta$ (see Fig.1(b) and Table I in Appendix C).

One can now interpret how the HF coupling leads to the raise of what we call the "chameleon" states and understand their distinction from the usual dark and bright states. The dark states can be easily identified via performing the MS transformation of the HF state vectors $|FM\rangle$ in the space Λ_f (see Fig.1(b) and Fig.4(b)); we denote the subspace of Λ_f formed by the set of "dark" basis vectors $|d_1\rangle, ..., |d_\kappa\rangle$ as Λ_f^{DS}. The subspace of bright states Λ_f^{BS} includes all those states that can be directly excited from the ground state by the P-laser field and that are coupled with their pre-image vectors $|i\rangle_{F''M}$ by the MS effective Rabi frequency $\Omega_{M_J}^{ef}$ with $M_J = 1/2$ (see Eq. (B3) in App. B).

The chameleon states are those state vectors in the f-space Λ_f with the basis set $|f_0\rangle, ..., |f_\chi\rangle$ that simultaneously satisfy two conditions: (1) they belong to a subspace Λ_f^{CS} that is orthogonal to both Λ_f^{DS} and Λ_f^{BS}, and (2) their pre-images $|i_0\rangle, ..., |i_\chi\rangle$, which constitute subspace Λ_i^{CS}, are orthogonal to all vectors $|i\rangle_{F''M}$. This means that even if coupling between the vectors $|i_r\rangle$ and $|f_r\rangle$ ($r = 0, ..., \chi$) by the S-laser field does lead to the formation of a pair of diverging adiabatic states $|r\rangle_\pm$ with energy separation that increases with $\Omega_{3/2}^{ef} \sim \Omega_S$, those states would normally not be excited by the P-laser field from state g if not for the hyperfine interaction in state i. Importantly, the HF interaction mixes the chameleon adiabatic states $|r\rangle_\pm$ with the bright states $|i\rangle_{F''M}$, enabling their excitation from state g by the P-laser field. For each set of states with a given M depicted in Fig.6(a)-(c), the number of chameleon states is obtained as difference between the number of components in the subspace $\Lambda_i(M)$ and the number of components in state g (see Table I in Appendix C).

The expression of chameleon states in the AT excitation spectra (see peaks $0_\pm$, in Fig.3, Fig.7, Fig.8) has the following distinct signature. Firstly, the peaks associated with the chameleon states behave essentially as those associated with bright states in terms of increasing separation between the peaks with increasing Ω_S. At the same time, as discussed in Sect. III C, the population sharing between bright and chameleon

states induced by the HF interaction decreases proportionally to Ω_S^{-2}, hence the peaks associated with the chameleon states will fade out with increasing Ω_S. A simple calculation presented in Appendix C for the case of $M = 1$ (see Fig.1(b)) gauges the involved HF interaction strengths. In particular, for the interaction between the bright state $|i\rangle_2$ and the chameleon state $|i_0\rangle$ one finds $\varpi_I = \langle i_0|\hat{H}^h|i\rangle_2 = 28.5$MHz; this is the interaction that leads to visualization of the otherwise forbidden transitions to chameleon states that give rise to peaks $0_\pm$ in Figs. 3,7,8.

The above presented systematization of adiabatic states allows one also to explain the complementarity of peaks $1_\pm$, $2_\pm$ in the AT spectra for the $M = 1$ sequence shown in Fig.8 upon excitation from the $F'' = 1$ and $F'' = 2$ HF components of the ground state, respectively. Coupling with the S-laser field leads to formation of two bright states, $|f\rangle_1$ and $|f\rangle_2$, in the subspace Λ_f^{BS}. Because of the specific features of the excitation scheme of Fig.1(b), the state $|f\rangle_1$ is populated upon excitation of the $3s_1/2, F''=1 \to 3p_{3/2}$ transition by the P-laser field, giving raise to peaks $1_\pm$ in Fig.8(a), while excitation of the $3s_1/2, F''=2 \to 3p_{3/2}$ transition leads to population of $|f\rangle_2$ that gives raise to peaks $1_\pm$ in Fig.8(b). Note, that for this selectivity to be valid it is not required for the spectral lines associated with the BS $|f\rangle_1$ and $|f\rangle_2$ to be resolved. Hence, by a proper choice of the initial HF state in level g it is possible to selectively address different unresolved HF components in state f if a strong laser field is coupled between levels i and f.

Care must be taken when extending the above analysis to other excitation schemes involving different level systems and/or laser polarizations, because those will usually produce different sets of adiabatic states. For example, the AT spectra presented in Fig.7 and Fig.8 may create the impression that only the outermost pair of peaks with the largest energy separation survives at very large Ω_S. However, if the $4d_{5/2}$ state in Fig.1 was replaced by $4d_{3/2}$, only the two innermost peaks would survive the increase of Ω_S. The choice of laser field polarizations significantly affects the AT spectra, too. In our study, we considered the case of linearly polarized P- and S-laser fields, which results in a twofold degeneracy of adiabatic states for $|M| > 0$ since in this case Rabi frequencies do not depend on the sign of M. Application of circularly polarized laser light lifts this degeneracy and leads to richer AT spectra.

VI. CONCLUSIONS

We have studied the formation of adiabatic states in multi-level systems that exhibit non-negligible HF interaction. We have shown that at strong laser coupling associated with large Rabi frequencies Ω_S the HF interaction operator $\hat{H}^h$ can be treated as a perturbation in the basis of adiabatic states formed by the light-atom coupling operator $\hat{V}$ due to the interaction of atoms with the strong laser field. By analyzing the AT spectra in Na atoms obtained by scanning a weak probe laser field across the $3s_{1/2}(F''=1,2) \to 3p_{3/2}$ transition that excites the adiabatic states formed upon coupling a strong S-laser field between the $3p_{3/2}$ and $4d_{5/2}$ states, we reach the following conclusions:

(i) a strong laser coupling produces the usual bright (coupled) and dark (uncoupled) states, and a third kind of states - the chameleon states that belong to the subspace Λ_f^{CS} of space Λ_f that is orthogonal to both the subspace of dark states Λ_f^{DS} and the subspace of bright states Λ_f^{BS} (see Fig.1(b)). In terms of energy dependence, pairs of coupled chameleon states behave as pairs of bright states, with the energy separations between the respective $|+\rangle$ and $|-\rangle$ components of the chameleon pair increasing proportional to Ω_S. While they are nominally "dark" with respect to excitation by the probe field, the perturbation introduced by the HF interaction can lift this restriction. At moderate Ω_S, when $\hat{V}$ is comparable to $\hat{H}^h$, the chameleon states are well observed in the AT spectrum and they exhibit features typical of bright states. As Ω_S becomes much larger than the energy of the HF interaction, the effect of the latter dwindles and the chameleon states gradually vanish from the excitation spectrum similarly to dark states in the example of Fig.2, albeit with energy separation between the components of the chameleon pair keeping to increase with Ω_S. This is reflected by the behavior of peaks 0_+, 0_- in the AT spectra presented in Fig.7;

(ii) when the adiabatic states are probed from either the $F'' = 1$ or $F'' = 2$ HF level of the ground state, one is in fact addressing independent (orthogonal) sets of adiabatic states representing separate three-level ladder-like sequences (see Eq.(22)) — one set is selectively excited from $F'' = 1$, and a different set from $F'' = 2$. As we demonstrate in Fig.8 on the example of the ladders of HF levels with $|M| = 1$ probed from either $F'' = 1$ or $F'' = 2$, those orthogonal sets can be composed of different excited HF sublevels. For this selectivity to be valid, it is not required that the respective spectral lines are resolved.

The latter conclusion is not only of purely academic interest. Provided a suitable energy level system, it can be used to achieve a selective excitation of unresolved excited states, such as HF levels of Rydberg atoms. One can extend this way of thinking to develop more general schemes for laser-induced adiabatic state engineering that utilizes manipulation of two-photon selection rules to achieve control of quantum state populations with high fidelity. The discussion of such schemes goes beyond the scope of this paper and it shall be a subject of another forthcoming publication.

ACKNOWLEDGMENTS

This work was supported by the U.S. Office of Naval Research under Grant No.N00014-12-1-0514. Partial support by the EU FP7 Centre of Excellence FOTONIKA-LV (T.K. and N.N.B.), EU FP7 IRSES project NOCTURNAL ATMOSPHERE (K.M.), and the trilateral grant FP-20338-ZF-N-100 by the Latvian, Lithuanian, and Taiwanese Research Councils (T.K., A.C., and M.A.) are also acknowledged. We wish to thank Klass Bergmann and Bruce W. Shore for helpful discussions at the early stages of the work presented here.

Appendix A: Treatment of perturbation by HF interaction using the projection operators' technique

Consider the MS states shown in Fig.5(b). One can introduce in space $\Lambda = \Lambda_B \oplus \Lambda_A$ the projection operators $\hat{P}_\pm$ and $\hat{P}_D$ that act in a two-dimensional subspace of two coupled states $\Lambda^\pm = \{|i\rangle, |Br\rangle\}$ and in a $\kappa = (N_B - 1)$-dimensional subspace of dark states $\Lambda^D = \{|d_r\rangle\}$ ($r = 1, ..., \kappa$), respectively:

$$\hat{P}_\pm = |Br\rangle\langle Br| + |i\rangle\langle i|, \tag{A1}$$

$$\hat{P}_D = \hat{I} - \hat{P}_\pm = \sum_r |d_r\rangle\langle d_r|. \tag{A2}$$

The Hamiltonian of the HF interaction can then be written as

$$\hat{H}^h = \left(\hat{P}_\pm + \hat{P}_D\right) \hat{H}^h \left(\hat{P}_\pm + \hat{P}_D\right). \tag{A3}$$

The aggregate Hamiltonian $\hat{H}^s$ (1) in the $\Im_{MS}$ basis can now be reduced to the following form:

$$\hat{H}^s = \hat{H}_{MS} + \hat{H}_{\pm D} + \hat{H}_{D\pm}; \tag{A4}$$

$$\hat{H}_{MS} = \begin{pmatrix} 0 & \Omega_{Br}/2 & 0 \\ \Omega_{Br}/2 & \langle Br|\hat{H}^h|Br\rangle & 0 \\ 0 & 0 & \hat{P}_D\hat{H}^h\hat{P}_D \end{pmatrix}; \tag{A5}$$

$$\hat{H}_{\pm D} = \hat{P}_\pm \hat{H}^h \hat{P}_D; \quad \hat{H}_{D\pm} = \hat{P}_D \hat{H}^h \hat{P}_\pm. \tag{A6}$$

The eigenfucntions of the operator $\hat{H}_{MS}$ correspond to adiabatic states in space Λ in the limit of strong coupling $\Omega_{Br} \gg \Delta_\gamma$. From the above representation of $\hat{H}^s$ one can infer the following.

(i) The operator $\hat{P}_\pm \hat{H}^h \hat{P}_\pm$ entering $\hat{H}_{MS}$ as a "diagonal element" in the first two lines/rows is responsible for the energy shift Δ_{Br} of the bright state $|Br\rangle$ that is illustrated in Fig.5(b) (see also Eq.(11)). The diagonalization of such two-dimensional matrix is a well known problem, the solution of which yields in subspace $\Lambda^\pm$ two adiabatic states $|+\rangle, |-\rangle$ with energies $\varepsilon_\pm$, whereby the former are linear combinations of states $|Br\rangle$ and $|i\rangle$ (see Eq. (12)) [16].

(ii) The operator $\hat{P}_D \hat{H}^h \hat{P}_D$ of $\hat{H}_{MS}$ is a $(N_A - 1)$-dimensional matrix acting in the subspace of dark states Λ^D. Its diagonalization results in new dark states $|D_r\rangle$ with energy splittings ε_r between the adjacent states (see Fig.5(c)). Following the methodology developed in [6], one can show that the regular sequence of dark state energies $\{\varepsilon_r\}$ ($\varepsilon_1 < \varepsilon_2 < \cdots < \varepsilon_{N_A-1}$) is slightly shifted with respect to the diabatic state energies $\{\Delta_\gamma\}$ (see Eq.(14)).

(iii) The operators $\hat{H}_{\pm D}, \hat{H}_{D\pm}$ introduce mixing between the subspaces $\Lambda^\pm$ and Λ^D. At $\Omega_{Br} \gg |\Delta_\gamma|$ the energy separation between the states belonging to different subspaces $\Lambda^\pm$ and Λ^D is accordingly large: $|\varepsilon_\pm - \varepsilon_r| \sim \Omega_{Br}/2$. This has two consequences. First, the perturbations $\delta\varepsilon_\pm$ and $\delta\varepsilon_r$ of the zero-order adiabatic energies $\varepsilon_\pm$ (Eq.(13)) and ε_r (Eq.(14)) are determined by the "two-photon" matrices $\hat{\Pi}_\pm \simeq 2\hat{H}_{\pm D}\hat{H}_{D\pm}/\Omega_{Br}$ and $\hat{\Pi}_D \simeq 2\hat{H}_{D\pm}\hat{H}_{\pm D}/\Omega_{Br}$ acting within the subspaces $\Lambda^\pm$ and Λ^D, respectively [22]. The magnitude of these perturbations can be estimated as $|\delta\varepsilon_\pm| < 2\max\left(|\Delta_\gamma|\right)^2/\Omega_{Br}$, $|\delta\varepsilon_r| < 2\,|\varepsilon_r| \cdot \max\left(|\Delta_\gamma|\right)/\Omega_{Br}$, i.e. they are very small in the limit of large Ω_{Br}. Second, the mixing introduced by $\hat{H}_{\pm D}, \hat{H}_{D\pm}$ leads to population sharing between the bright and dark states. Since $\left|\langle \pm|\hat{H}_{\pm D}|D_r\rangle\right| < \max\left(|\Delta_\gamma|\right)$, the relative population $P_\pm$ of bright states in the dark subspace Λ^D does not exceed the value given by Eq.(15) (see [29], Chapt. VI).

Appendix B: The basis of broken-down HF coupling

When the HF coupling is broken down due to interaction with the S- (or P-) laser field, the HF basis is no longer valid. Under such conditions we rely on the fine structure basis that uses the product $|LJM_JM_I\rangle = |LJM_J\rangle|M_I\rangle$ of basis vectors of electron $|LJM_J\rangle$ and nuclear spin $|M_I\rangle$. This basis is useful for the construction of adiabatic states at large $\Omega_S \gg 110$MHz, when coupling with the S-laser field breaks down the HF interaction in the $3p_{3/2}$ state, and it also provides some useful insights into the properties of adiabatic states formed in the excitation scheme presented in Fig.1(a).

The Rabi frequencies of the transitions $\{LJM_JM_I \to \tilde{L}\tilde{J}\tilde{M}_J\tilde{M}_I\}$, whereby linear laser polarizations imply that $\tilde{M}_J = M_J$, $\tilde{M}_I = M_I$, are given by [36]

$$\Omega^{(LJ)}_{\tilde{L}\tilde{J}}(M_J) = \langle \tilde{L}\tilde{J}M_JM_I|E_\kappa \hat{d}_z|LJM_JM_I\rangle = (-1)^\Phi \Omega_\kappa \times \begin{Bmatrix} L & J & s \\ \tilde{J} & \tilde{L} & 1 \end{Bmatrix} \sqrt{(2\tilde{J}+1)(2J+1)} \begin{pmatrix} J & 1 & \tilde{J} \\ -M_J & 0 & M_J \end{pmatrix}, \tag{B1}$$

where phase $\Phi = \tilde{L} + s + 1 + \tilde{J} + J - M_J$ ($s = 1/2$ is the electron spin), the index κ stands for the P- or S-laser excitation, $M_J = -J, -J+1, \ldots, J$, and $M_I = -I, -I+1, \ldots, I$.

The equation (B1) has an important implication that both laser fields couple only the levels with the same quantum numbers M_J, M_I. This means that the linkage diagram shown in Fig.1(a) can be simplified to a set of

TABLE I. Coefficients $C_{F'}$ for representations of bright-states $|i\rangle_\eta$ and chameleon-states $|i_\chi\rangle$ in the HF basis for manifolds with different M.

$M=0$

States	C_0	C_1	C_2	C_3
$\|i\rangle_2$	0	-0.31623	0	0.94868
$\|i\rangle_1$	-0.70711	0	0.70711	0
$\|i_0\rangle$	0	0.94868	0	0.31623
$\|i_1\rangle$	0.70711	0	0.70711	0

$M=\pm1$

States	C_1	C_2	C_3
$\|i\rangle_2$	-0.27386	-0.35355	0.89443
$\|i\rangle_1$	-0.79057	0.61237	0
$\|i_0\rangle$	0.54772	0.70711	0.44721

$M=\pm2$

States	C_2	C_3
$\|i\rangle_2$	-0.70711	0.70711
$\|i_0\rangle$	0.70711	0.70711

separate noninteracting three-level ladders

$$\left|3s_{1/2}M_J\right\rangle \rightarrow \left|3p_{3/2}M_J\right\rangle \rightarrow \left|4d_{5/2}M_J\right\rangle, \tag{B2}$$

similar to those depicted in Fig.1(b). Importantly, equation (B1) determines the effective MS frequencies Ω_χ^{ef} of the operator $\hat{V}_S=-E_S\hat{d}_z$. Since the value of Ω_χ^{ef} does not depend on the sign of M_J [35], it can take only two possible values depending on whether $|M_J|=1/2$ or $3/2$:

$$\Omega^{ef}_{1/2,3/2}\equiv\Omega^{(lJ)}_{\tilde{l}\tilde{J}}(M_J=1/2,3/2), \tag{B3}$$

where the ratio $\Omega^{ef}_{1/2}/\Omega^{ef}_{3/2}=\sqrt{1.5}$ [35]. The value $\Omega^{ef}_{1/2}$ is associated with the excitation ladder scheme (B2) for $M_j=1/2$ and, consequently, relates to the effective MS Rabi frequencies of bright states in Fig.1(b). On the other hand, the coupled levels $\left|3p_{3/2}M_j=3/2\right\rangle$, $\left|4d_{5/2}M_j=3/2\right\rangle$ are impossible to excite by the P-laser from $\left|3s_{1/2}M_j=1/2\right\rangle$ state, i.e., $\Omega^{ef}_{3/2}$ relates to the chameleon states in Fig.1(b).

Appendix C: Hyperfine operator in the Morris-Shore basis

Consider the MS basis for states presented in Fig.1(b) for a given fixed value of M. Explicit representation of the bright states $|i\rangle_\eta$ in the HF basis $|F'M\rangle$ of the $3p_{3/2}$ state subspace $\Lambda_i(M)$,

$$|i\rangle_\eta=\sum C_{F'}|F'M\rangle, \tag{C1}$$

can be found by rewriting Eq. (22) in the form

$$|i\rangle_{F''M}=\sum_{F'}|F'M\rangle\langle F'M|\hat{V}_P|F''M\rangle, \tag{C2}$$

TABLE II. Matrix elements of the HF operator in the MS basis for $M=1$, in units of MHz.

States	$\|i\rangle_2$	$\|i\rangle_1$	$\|i_0\rangle$
$\|i\rangle_2$	44.650	-7.3612	28.700
$\|i\rangle_1$	-7.3612	-21.250	14.722
$\|i_0\rangle$	28.700	14.722	1.6000

whereby matrix elements of the operator $\hat{V}_P$ of the interaction of atoms with the P-laser field are well known [36]:

$$\langle 3p_{3/2}F'M|E_P\hat{d}_z|3s_{1/2}F''M\rangle=\sqrt{(2F''+1)(2F'+1)}\times$$
$$\Xi(-1)^{F''+F'-M}\begin{Bmatrix}1/2 & F'' & 3/2\\ F' & 3/2 & 1\end{Bmatrix}\begin{pmatrix}F'' & 1 & F'\\ -M & 0 & M\end{pmatrix}, \tag{C3}$$

where Ξ is a constant the exact value of which is of no further significance to the discussion in this section.

Table I lists the values of the coefficients $C_{F'}$ entering Eq. (C1) for normalized bright and Chameleon states. The number of bright states varies for different M manifolds:

(i) for $M=0$ and $F'=0,1,2,3$ (see Fig.6(b)) there are two bright states ($\eta=2,1$) in the four-dimensional HF subspace $\Lambda_i(M)$;

(ii) for $M=\pm1$ and $F'=1,2,3$ there are two bright states ($\eta=2,1$) in each of the three-dimensional subspaces $\Lambda_i(M)$ with $M=+1$ and $M=-1$;

(iii) for $M=\pm2$ and $F'=2,3$ there is a single bright state ($\eta=2$) in each of the two-dimensional subspaces $\Lambda_i(M)$ with $M=+2$ and $M=-2$.

The normalized chameleon states $|i_\chi\rangle$ are found as those state vectors that are orthogonal to all bright states $|i\rangle_\eta$ in the subspace $\Lambda_i(M)$.

In the HF basis $|F'\rangle\equiv|F'M\rangle$ of Fig.6(b), the operator $\hat{H}^h$ (measured in MHz) has the following diagonal representation that is determined by the HF splittings of the $3p_{3/2}$ state (see Fig.1(a)):

$$\hat{H}^h=58.3|F'=3\rangle\langle F'=3|-34.3|F'=1\rangle\langle F'=1|. \tag{C4}$$

The values of matrix elements of the HF operator $\hat{H}^h$ in the MS basis $\{|i\rangle_2,|i\rangle_1,|i_0\rangle\}$ ($M=1$) are listed in Table II. The diagonal elements of the table give the shifts of the MS state energies, while the off-diagonal elements are frequencies ϖ of mixing between the MS states induced by the HF interaction. The strongest mixing ($\varpi=28.7$ MHz) occurs between the bright state $|i\rangle_2$ and the chameleon $|i_0\rangle$, which has motivated our choice of the simplified model excitation scheme shown in Fig.3. In order to more clearly demonstrate the effect of elimination of chameleon peaks $0_\pm$ from the AT spectra upon increasing Ω_S, the spectra presented in Fig.3 have been obtained using the following, somewhat modified, model

parameter values: $\varpi_I = 50$MHz for the HF induced mixing frequency (instead of 28.7MHz from Table II) and $\Delta\varepsilon_{20} = 30$MHz for the energy splitting between the $|i\rangle_2$ and $|i_0\rangle$ states (instead of 43.1MHz from Table II).

[1] J. R. Morris and B. W. Shore, Phys. Rev. A **27**, 906 (1983).
[2] S. H. Autler and C. H. Townes, Phys. Rev. **100**, 703 (1955).
[3] F. Paschen and E. Back, Physica **1**, 261 (1921).
[4] G. W. Drake, *Springer Handbook of Atomic, Molecular, and Optical Physics*, Springer Handbook of Atomic, Molecular, and Optical Physics (Springer, 2006).
[5] M. Auzinsh, D. Budker, and S. M. Rochester, Phys. Rev. A **80**, 053406 (2009).
[6] U. Fano, Phys. Rev. **124**, 1866 (1961).
[7] G. Alzetta, A. Gozzini, L. Moi, and G. Orriols, Il Nuovo Cimento B Series 11 **36**, 5 (1976).
[8] S. E. Harris, J. E. Field, and A. Imamoglu, Phys. Rev. Lett. **64**, 1107 (1990).
[9] L. V. Hau, S. E. Harris, Z. Dutton, and C. H. Behroozi, Nature **397**, 594 (1999).
[10] M. M. Kash, V. A. Sautenkov, A. S. Zibrov, L. Hollberg, G. R. Welch, M. D. Lukin, Y. Rostovtsev, E. S. Fry, and M. O. Scully, Phys. Rev. Lett. **82**, 5229 (1999).
[11] C. Liu, Z. Dutton, C. H. Behroozi, and L. V. Hau, Nature **409**, 490 (2001).
[12] D. F. Phillips, A. Fleischhauer, A. Mair, R. L. Walsworth, and M. D. Lukin, Phys. Rev. Lett. **86**, 783 (2001).
[13] L.-M. Duan, M. D. Lukin, J. I. Cirac, and P. Zoller, Nature **414**, 413 (2001).
[14] H. Lee, M. Fleischhauer, and M. O. Scully, Phys. Rev. A **58**, 2587 (1998).
[15] J. Kitching, S. Knappe, and L. Hollberg, Appl. Phys. Lett. **81**, 553 (2002).
[16] K. Bergmann, H. Theuer, and B. W. Shore, Rev. Mod. Phys. **70**, 1003 (1998).
[17] N. V. Vitanov, A. A. Rangelov, B. W. Shore, and K. Bergmann, Rev. Mod. Phys. **89**, 015006 (2017).
[18] S. Stenholm, *Foundations of Laser Spectroscopy*, ISBN: 0486444988 (Courier Dover Publications, 2005).
[19] J. Qi, G. Lazarov, X. Wang, L. Li, L. M. Narducci, A. M. Lyyra, and F. C. Spano, Phys. Rev. Lett. **83**, 288 (1999).
[20] A. A. Rangelov, N. V. Vitanov, and B. W. Shore, Phys. Rev. A **74**, 053402 (2006).
[21] S. Reynaud and C. Cohen-Tannoudji, J. Phys. France **43**, 1021 (1982).
[22] B. W. Shore, *Manipulating quantum structures using laser pulses* (Cambridge University Press, 2011).
[23] I. Sydoryk, N. N. Bezuglov, I. I. Beterov, K. Miculis, E. Saks, A. Janovs, P. Spels, and A. Ekers, Phys. Rev. A **77**, 042511 (2008).
[24] N. Porfido, N. N. Bezuglov, M. Bruvelis, G. Shayeganrad, S. Birindelli, F. Tantussi, I. Guerri, M. Viteau, A. Fioretti, D. Ciampini, *et al.*, Physical Review A **92**, 043408 (2015).
[25] M. Bruvelis, A. Cinins, A. Leitis, D. Efimov, N. Bezuglov, A. Chirtsov, F. Fuso, and A. Ekers, Optics and Spectroscopy **119**, 1038 (2015).
[26] S. A. Kandela, Appl. Opt. **23**, 2152 (1984).
[27] U. Volz, M. Majerus, H. Liebel, A. Schmitt, and H. Schmoranzer, Phys. Rev. Lett. **76**, 2862 (1996).
[28] M. Auzinsh, N. N. Bezuglov, and K. Miculis, Phys. Rev. A **78**, 053415 (2008).
[29] L. D. Landau and E. M. Lifshitz, *Quantum Mechanics: Non-Relativistic Theory*, ISBN: 0750635398 (Butterworth-Heinemann, 1981).
[30] G. Vasilev and N. Vitanov, arXiv preprint arXiv:1402.5673 (2014).
[31] F. Bloch, Phys. Rev. **70**, 460 (1946).
[32] A. K. Kazansky, N. N. Bezuglov, A. F. Molisch, F. Fuso, and M. Allegrini, Phys. Rev. A **64**, 022719 (2001).
[33] N. N. Bezuglov, R. Garcia-Fernandez, A. Ekers, K. Miculis, L. P. Yatsenko, and K. Bergmann, Phys. Rev. A **78**, 053804 (2008).
[34] D. K. Efimov, N. N. Bezuglov, A. N. Klyucharev, Y. N. Gnedin, K. Miculis, and A. Ekers, Optics and Spectroscopy **117**, 8 (2014).
[35] I. I. Sobelman, *Atomic Spectra and Radiative Transitions*, ISBN: 978-3-642-76907-8 (Springer, 1992).
[36] M. Auzinsh, D. Budker, and S. Rochester, *Optically Polarized Atoms (Understanding light-atom interactions)*, ISBN: 0199565120 (Oxford University Press, 2010).
[37] M. Bruvelis, J. Ulmanis, N. N. Bezuglov, K. Miculis, C. Andreeva, B. Mahrov, D. Tretyakov, and A. Ekers, Phys. Rev. A **86**, 012501 (2012).